A Polydiacetylene in Dilute Solution

Renliang Xu† and Benjamin Chu*,†,‡

Departments of Chemistry and Materials Science and Engineering, State University of New York at Stony Brook, Long Island, New York 11794-3400. *Received November 7, 1988; Revised Manuscript Received December 21, 1988*

ABSTRACT: Laser light scattering (LLS), transient electric birefringence (TEB), and optical absorption were used to study polydiacetylene P4BCMU (poly[1,2-bis[4-[[[(2-butoxy-2-oxoethyl)amino]carbonyl]oxy]-butyl]-1-buten-3-yne-1,4-diyl]) in dilute chloroform/toluene solutions with various solvent compositions. Two different molecular weight P4BCMU samples were investigated. P4BCMU molecules in chloroform are wormlike coils with an average persistence length of ~16 nm. When the mole fraction of chloroform in a chloroform/toluene mixture is smaller than ~0.4, P4BCMU molecules in dilute solutions form aggregates, with molecular weight and size varying according to the solvent composition. Profile analysis of autocorrelation functions yields a broad size distribution when P4BCMU is dissolved in chloroform. However, much narrower size distributions are found once the aggregates are formed. Various models are applied to fit the experimental results, yielding mostly fairly stiff rodlike structures for the aggregates. The aggregation mechanism is discussed.

I. Introduction

Polydiacetylenes, $(=CR—C\equiv C—CR'=)_n$, polydiacetylene and its derivatives, are prototype conducting polymers[1] and can be used as a new class of electronic materials. They have been available since the late 1960s with the solid-state 1,4-addition polymerization of substituted diacetylenes.[2] Most polydiacetylenes are insoluble even in exotic solvents and infusible because of their rotation-restricted stiff backbone.[3] After the first soluble polydiacetylene, P*n*BCMU, in which R′ = R = $(CH_2)_nOCONHCH_2COOC_4H_9$, was synthesized a decade ago,[4] there have been extensive studies on the electronic, optical, mechanical, and conformational properties of polydiacetylenes in both solid (crystals and thin films) and liquid (gels and solutions) states. This research topic has also been the subject of several books.[5-8]

Applications of polydiacetylenes in materials science have become significant because of their many interesting properties, such as the large quasi-one-dimensional structure of their single crystals, the high third-order optical susceptibility, the large optical nonlinearity, and the high photoconductivity.[9-11] The color change of polydiacetylenes associated with either the solid-state polymerization by γ-radiation or the conformational change can be used to monitor any one of the following ambient parameters: time–temperature exposure, humidity, pressure, radiation exposure, pH, and gas exposure. Commercial products that try to take advantage of the color change are time–temperature and radiation dosage indicators consisting of a diacetylene ink printed as a bar-code label of the type commonly used for automatic product identification and pricing in merchandising, but providing dynamic instead of static information.[12-13] Polydiacetylenes have been used as a film waveguide in interferometers.[14-15] The potential use of polydiacetylenes as an optical memory and information processor has also been explored.[16]

The unique property to which most attention has been paid is the peculiar color change of polydiacetylenes in solution at different temperatures or at different solvent conditions; e.g. solutions of P4BCMU in toluene at room temperature are red and will gradually turn to yellow by adding chloroform or by raising the temperature. Over 20 major techniques, e.g. nuclear magnetic resonance, Fourier transform infrared spectroscopy, viscoelastic measurements, light scattering, transient electric birefringence, optical Kerr effect, and Raman and absorption spectroscopy, which cover a broad detection region from picosecond to millisecond in time and from angstrom to micrometer in space, have been applied to study the dramatic color change of more than 10 members, e.g. P*n*BCMU and PTS12 (R = $(CH_2)_4OSO_2BzCH_3$), of the soluble polydiacetylene family.[17-27]

Customarily known as P4BCMU ($(C_{26}H_{40}N_2O_8)_n$, M_{mono} = 508 g/mol, L_{mono} = 4.8 Å[26], poly[5,7-dodecadiyne-1,12-bis[[(4-butoxycarbonyl)methyl]urethane]], or systematically named poly[1,2-bis[4-[[[(2-butoxy-2-oxoethyl)-amino]carbonyl]oxy]butyl]-1-buten-3-yne-1,4-diyl], was first synthesized in 1978.[4] It has bulky, sufficiently flexible and polar substituent groups R = $(CH_2)_4OCONHCH_2CO-OC_4H_9$. The backbone configuration of P4BCMU is believed to be a resonance mixture of two mesomeric structures, i.e. the favored acetylenic structure and the much less favored butatrienic structure (ref 16 and references therein):

$$(=RC—C\equiv C—CR=)_n \leftrightarrow (-RC=C=C=CR-)_n$$

It should be noted that the existence of the butatrienic form is being disputed.

The crystal of P4BCMU has a quasi-one-dimensional structure because of the conjugated backbone. P4BCMU is highly soluble in chloroform (>5%) and forms a yellow solution with a blue shift in the optical absorption peak from $\lambda_{max} \approx 625$ nm of the original crystalline state[28] to $\lambda_{max1} \approx 460$–470 nm. Dramatic reversible color change—from yellow to red with an additional absorption at $\lambda_{max2} \approx 520$–550 nm—occurs by adding *n*-hexane (a nonsolvent) to P4BCMU/$CHCl_3$ solution.[19] Subsequent addition of *n*-hexane results in the precipitation of the polymer as a red solid. The precipitation process varies considerably with polymer concentration, while the conformational transition (the color change) occurs at a fixed $CHCl_3/C_6H_{14}$ ratio over a range of concentrations spanning 3 orders of magnitude from 3×10^{-3} to 1×10^{-5} g/mL. A similar phenomenon is observed when P4BCMU is dissolved in toluene (a poor solvent). At high temperatures, the solution is yellow, and at lower temperatures it becomes red. It has been found in many experiments that the size of P4BCMU molecules depends on solution color. Several theoretical models and calculations have been proposed to explain the phenomenon.[29-33] The focal points are the structures and transition mechanisms of polydiacetylenes in different environments. The conformation of soluble

* Author to whom all correspondence should be addressed (use Department of Chemistry).
† Department of Chemistry.
‡ Department of Materials Science and Engineering.

0024-9297/89/2222-3153$01.50/0

polydiacetylenes in good solvent is clear; i.e., they are wormlike coils of small overall size (a few hundred angstroms) with a fairly broad size distribution. But how are the coils being transformed to another state and what is the other state when the solvent condition becomes poorer? What is the relation between the electronic configuration, which displays the color, and the geometric conformation, which determines the particle size and shape? We shall attempt to answer those questions in this article.

Transient electric birefringence (TEB), as an important branch of modern electrooptics, with single, reversed or sinusoidal electric pulses has become a useful tool for studying the structure and the electrical, optical, and hydrodynamic properties and particle sizing of large anisotropic particles in solution (or suspension). TEB can determine the rotational diffusion coefficient and obtain information about the optical anisotropy of particles.

From fluctuations of the dielectric constant, density or concentration of the scattering medium, laser light scattering (LLS) detects the scattered electric field, which results from the interaction of molecules with the incident light, as functions of time and space to obtain information on the structures, e.g. the z-averaged radius of gyration (R_g), the weight-averaged molecular weight (M_w), and the second virial coefficient (A_2), and on the translational as well as internal motions, e.g. the z-averaged translational diffusion coefficient (D_T) and the rotational diffusion coefficient (D_R), of the scattering particles in solution (or suspension).

In the present study LLS is used to study P4BCMU in mixed solvents of chloroform/toluene as functions of time and solvent composition. Optical absorption monitors the time and composition dependence of the solvatochromic transition. TEB is also employed to determine the amplitudes of the solution birefringence and particle rotational diffusion coefficient. The molecular status and possible transition mechanisms are then drawn from the results of data analysis.

Our studies on P4BCMU in chloroform/toluene dilute solutions as functions of time and composition show that coils of P4BCMU in relatively good solvents could become rodlike aggregates when the solvent condition becomes poorer. The transition happens when the mole fraction of chloroform in the solvent mixture is less than ~0.4; it takes a short time period (<1 h) to form aggregates, while much longer time is needed for the whole solution to reach a stationary state.[34] The size of the aggregate depends on the solvent composition and the polymerization number of P4BCMU. In pure toluene solution the average aggregation numbers are 360 and 14 for P4BCMU samples of molecular weight $M_w = 1.2 \times 10^5$ and 2.4×10^6 g/mol, respectively. The aggregation process might be stimulated from the charge transfer of the polymer chain with the solvent.[35] A reciprocal relation between the average aggregation number and the weight-average molecular weight was observed.

II. Experimental Aspects

II.1. Sample and Solution Preparations. The experiments involve two P4BCMU samples, which were obtained courtesy of Drs. R. R. Chance and D. G. Peiffer at Exxon Research and Engineering Co. The samples were used without further purification. We denote the two samples as sample A and sample B. Sample A was aged 3 years in a sealed bottle at room temperature.

Both samples were prepared[36] by a synthetic route similar to the one reported by Patel et al.[37] 5-Hexyn-1-ol, obtained from Farchan Research Laboratories, was oxidatively coupled 2 days either by Hay's method using copper(I) and tertiary amine as catalyst and oxygen gas as oxidation agent or by a stoichiometric oxidation procedure using copper(II) in pyridine/methanol/ether (1:1:4) solution. The product diacetylene diol was then reacted with n-butyl isocyanatoacetate in the dibutyltin bis(2-ethylhexanoate) and triethylamine catalyst system to obtain the desired diacetylene diurethane monomer. Further purification was carried out by recrystallization of monomer in an acetone/hexane mixed solvent.

The solid-state 1,4-addition polymerization of diacetylene units was initiated by γ-radiation (15-Mrd dose for sample A and 20-Mrd dose for sample B). Hot chloroform/hexane (in the case of sample A) or hot acetone (in the case of sample B) was used to wash the raw polymers and to remove unreacted monomers and oligomers. Pure polydiacetylenes were subtracted by filtration and nitrogen-flow drying. The polydiacetylene structures were reconfirmed by ^{13}C NMR spectra.

Solvents chloroform (used as a good solvent) and toluene (used as a poor solvent) of HPLC grade purchased from Fisher Scientific Co. were further purified by distillation.

The solution preparation was the same for all but the solution in pure toluene. Golden red P4BCMU solid was first dissolved in a small amount of chloroform. The dissolution was almost instantaneous for sample A and took a few minutes for sample B to form yellow solutions. This process could be easily visualized by associated color changes. Chloroform and toluene were then added to reach the desired solvent composition and concentration. For preparing a P4BCMU solution with pure toluene as the solvent, the solution bottle was kept in an oven at a temperature of about 70 °C with occasional stirring until the polymer was fully dissolved.

Since the sizes of P4BCMU polymer in solution change with solvent composition and concentration, the regular filtration procedure for solution clarification in LLS experiment was not adopted. It is difficult to choose a right pore size for the filter, and there is a possibility for shear-induced aggregation if the solution passes through the filter too fast. Instead, centrifugation with various centrifuging speeds was used to clarify the solutions for LLS measurements. Performed by a Sorvall Superspeed RC2-B centrifuge, the selected rotating speed was high enough to remove all foreign particles that would affect LLS measurements (residual of foreign dust particles could be visually checked in a laser beam) but low enough not to precipitate out any P4BCMU polymer (red precipitates on the wall of the centrifuge tube). Typical values of centrifuging force used were $1.2 \times 10^4 g$ for P4BCMU in chloroform and ~150g for most of the other solutions in a time period of 2–3 h. The centrifuged solutions were then transferred to cylindrical dust-free LLS cells with a diameter (o.d.) of 1 cm. In birefringence and absorption spectrum measurements the centrifugation procedure was not necessary. All of the measurements were performed at room temperature (22–24 °C).

II.2. Instrumentation and Data Analysis Procedures. A laboratory-made, fully automated LLS apparatus with a 50-mW He–Ne laser operated at $\lambda_0 = 632.8$ nm as the light source was used to perform static and dynamic light-scattering measurements in a scattering angular range of 15–135°.[38] At $\lambda_0 = 632.8$ nm the solution absorption was negligible. The intensity–intensity autocorrelation data ($G^{(2)}(\tau)$) were recorded by a Brookhaven Instruments BI2030AT 136 channel correlator, and the scattered intensities were recorded by an HP5328 counter.

The unnormalized square electric field correlation function from the self-beating dynamic light-scattering measurement is

$$\left(\frac{G^{(2)}(\tau)}{A} - 1\right) \approx \beta\left(\left(\frac{I - I_0}{I}\right)|g^{(1)}(\tau)|\right)^2 = \beta\left(\left(\frac{I - I_0}{I}\right)\int_{\Gamma_{min}}^{\Gamma_{max}} G(\Gamma)e^{-\Gamma\tau}\,d\Gamma\right)^2 \quad (1)$$

with $g^{(1)}(\tau)$, I_0, I, τ, A, Γ, $G(\Gamma)$, and β being the normalized electric field correlation function, the solvent scattered intensity, the solution scattered intensity, the delay time, the base line, the characteristic linewidth, the normalized characteristic linewidth distribution function, and an instrument beating efficiency coefficient, respectively. Most correlation data were fitted by the cumulants method.[39] Others were fitted by using CONTIN[40] to explore the size distribution. In the limits of angular extrapolation

and concentration extrapolation, Γ is related to the translational diffusion coefficient D_T ($=\Gamma/K^2$, K is the scattering vector related to the scattering angle θ, the wavelength of light in vacuo λ_0, and the refractive index of the solution n by $K = 4\pi n \sin(\theta/2)/\lambda_0$), which is the primary parameter to be used in further analysis.

The scattered intensity data recorded from the static light-scattering experiment at small scattering angles obeys the relation

$$\frac{I_0}{I - I_0} \approx \frac{1}{HCM_w}\left(1 + \frac{1}{3}K^2\langle R_g^2\rangle_z + 2A_2M_wC\right) \quad (2)$$

with C, M_w, A_2, and $\langle R_g^2\rangle_z$ ($=R_g^2$ hereafter for simplicity) being the solution concentration, the weight-averaged molecular weight, the second virial coefficient, and the square z-averaged radius of gyration; H ($=4\pi^2n^2(\partial n/\partial C)_{T,P}^2R_0/(N_A\lambda_0^4)$) is an optical constant related to the refractive index increment $(\partial n/\partial C)_{T,P}$ ($=\delta n/\delta C$ hereafter for clarity), the Rayleigh ratio of solvent R_0, and Avogadro's number N_A. In a plot of reciprocal excess scattered intensity of an optically anisotropic solution versus $\sin^2(\theta/2)$ at finite concentrations an apparent radius of gyration R_g* and an apparent molecular weight M_w* can be obtained from the slope and the intercept. The values of R_g* and M_w* have to be corrected for concentration effect by concentration extrapolation and for molecular anisotropy δ' ($=(a - b)/(a + b)$, with a and b being the polarizabilities in directions along the symmetric axis and the transverse axis for cylindrical particles), which could be determined from depolarized light-scattering measurements.[41,42]

TEB measurements were performed by our automated TEB apparatus.[43] A 15-mW He–Ne laser with a vertically polarized light of $\lambda_0 = 632.8$ nm and a divergence of 1 mrd was the light source. After two high-quality Glan–Thompson polarizers (extinction ratio $<5 \times 10^{-5}$), whose axes were set 45° with respect to the horizon, the incident light was focused on a 1-cm² Beckman cell in which two platinum electrodes were inserted and spaced 0.3 cm apart by a Teflon spacer. A quarter wave plate, whose axis direction was coincident with the first two polarizers, together with another Glan–Thompson polarizer, whose axis was positioned at 135° with respect to the horizon, serves as the analyzer. An RCA 1P28 photomultiplier tube (PMT) and a preamplifier performed the light signal to electrical signal conversion to produce a voltage output. A Kepco BOP 1000M bipolar operational power supply/amplifier was the high-voltage pulse supplier. A Morrow Designs microprocessor controlled the square-pulse generation, data acquisition, transfer display, and storage through a Biomation Model 8100 dual-channel transient recorder, which received the transmitted intensity from the PMT and the applied field shape from the electrodes. It has been found that the P4BCMU polymer in poor solvent, such as toluene, will be deposited to the negative electrode.[35] All TEB data were recorded by applying the electric field only once in order to avoid concentration change and possible structure change.

The recorded time-dependent transmitted intensity $I_{tr}(t)$ from TEB measurements were converted to time-dependent optical retardation $\delta(t)$ ($=2\pi l\Delta n(t)/\lambda_0$, with l and $\Delta n(t)$ being, respectively, the effective electrode length and the solution birefringence) according to

$$I_{tr}(t) = JI_p \sin^2(\alpha + \delta(t)/2) + I_s \quad (3)$$

where I_p, I_s, J, and α are the incident light intensity polarized at 45° with respect to the horizon, the intensity of stray light including dark counts from the PMT, an intensity loss factor resulting from absorption, reflection, and scattering, and a deviation angle from the cross position of the last polarizer to increase the signal-to-noise ratio and to distinguish the sign of $\delta(t)$, respectively. The amplitude of optical retardation δ and the relaxation rate τ^{-1} ($=^1/_6D_R$, D_R being the rotational diffusion coefficient) of the field-free decay in TEB measurements are related[43]

$$\delta(t) = \delta_0 \exp(-t/\tau) = (4\pi^2\phi_2\Delta g\Phi l/\lambda_0 n)\exp(-t/\tau) \quad (4)$$

with ϕ_2, Φ, and Δg being the volume fraction of the anisotropic solute, an orientation function whose value approaches 1 in high fields, and the optical anisotropy factor of the solute.

The absorption spectra (absorbance A ($=\log(I_0/I_{tr})$)) from $\lambda_0 = 350$ nm to $\lambda_0 = 650$ nm were recorded by using a GCA/McPherson 700 Series double-beam UV–visible spectrophotometer with 1-cm² quartz Beckman cells. Pure chloroform was used as a reference.

Table I
Refractive Index Increment ($\partial n/\partial C$) of P4BCMU in Solution at 24 °C

solvent	wavelength, nm	$(\partial n/\partial C)$, mL/g	source
chloroform	633	0.122 ± 0.005	this work
toluene	633	0.242	25
chloroform	578	0.185	25

The two distinguishable absorption peaks (referred to as peaks 1 and 2), which correspond to two electronic configuration states, overlap each other. For optimum precision in simultaneous spectrophotometric determinations, we need to choose the characteristic wavelengths representing the two peaks where the overlap is a minimum in order to avoid the complicated decomposition procedure due to overlapping of peaks.[44] Practically $\lambda_1 = 450$ nm and $\lambda_2 = 540$ nm were chosen as the two wavelengths from which the characteristic absorption amplitudes were measured since the extinction ratios of peak 1 and peak 2 at $\lambda = 450$ nm and $\lambda = 540$ nm, i.e. $\epsilon_{540}^1/\epsilon_{540}^2$ and $\epsilon_{450}^2/\epsilon_{450}^1$, were close to zero.

II.3. Physical Constant Measurements. a. The refractive index (n_m) of mixed solvents as a function of mole fraction of chloroform in a chloroform/toluene mixture X_c is calculated according to the Gladstone–Dale equation[45]

$$n_m(X_c) = 1 + \rho_m(X_c)\left[\frac{w_1}{\rho_1}(n_1 - 1) + \frac{w_2}{\rho_2}(n_2 - 1)\right] \quad (5)$$

where $\rho_m(X_c)$, ρ_i, w_i, and n_i are the density of the mixed solvent, the density of (pure) solvent i, the weight fraction of solvent i, and the refractive index of solvent i, respectively. The densities of solvent mixtures were measured by using a volumetric method at 20 °C while ρ_i could be found in the handbook.[46] $\rho_m(X_c)$ in units of grams per milliliter can be formulated as

$$\rho_m(X_c) = 0.865 + 0.498X_c - 4.27 \times 10^{-4}X_c^2 + 0.127X_c^3 \quad (6)$$

$n_{CHCl_3}^{632}$ ($=1.4405 + 6.1 \times 10^{-4}(25 - t)$) and $n_{C_7H_8}^{632}$ ($=1.4903 + 6 \times 10^{-4}(25 - t)$) with t being the temperature in degrees Celsius were obtained from ref 45 after interpolating to $\lambda_0 = 632.8$ nm. The value $n_m(X_c)$ was checked once by using our prism-cell small-angle light-scattering instrument.[47,48]

b. Viscosities for various solvent mixtures were measured at 20.0 and 23.4 °C by using a Cannon Ubbelohde viscometer according to the Poisseuille equation, after a kinetic energy correction and an entrance correction

$$\eta = A\rho t - B\rho/t \quad (7)$$

with A and B being viscometer constants and t being the flow time. At 20 °C η_{X_c} could be formulated in units of centipoise by

$$\eta_{X_c}^{20} = 0.547 + 0.0857X_c - 0.0661X_c^2 \quad (8)$$

c. The refractive index increment ($\partial n/\partial c$) of the P4BCMU solution varies with solvent composition. A modified Brice–Phoenix BP-2000-V differential refractometer with a 3-mW He–Ne laser ($\lambda_0 = 632$ nm) as the light source was used to measure ($\partial n/\partial c$) of P4BCMU in chloroform. Aldrich gold label sodium chloride (NaCl) of purity 99.999% was used as the standard to calibrate the apparatus. The result is listed in Table I where a comparison has also been made with literature values measured at a different wavelength or in a different solvent.

III. Results

III.1. Time Dependence. During the process of sample preparation it was found that the color, as well as the scattered intensity and the solution birefringence of a prepared solution, would change continuously for days. The solution would finally reach a stable state. The time needed for a solution to reach the stationary state varied with solvent composition. By tracing the absorption maximum at $\lambda_0 \approx 540$ nm as a function of time, we found it was slowest when chloroform and toluene were compe-

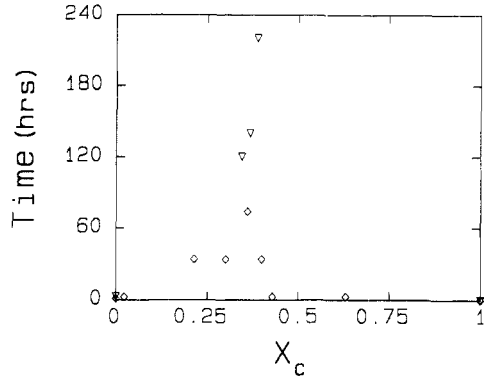

Figure 1. Time needed for various P4BCMU solutions to reach a stationary state as monitored by absorbance A_{540}. Diamonds for sample A ($M_w = 1.2 \times 10^5$ g/mol) and inverted triangles for sample B ($M_w = 2.4 \times 10^6$ g/mol). The concentration range was from 1×10^{-6} to 3×10^{-5} g/mL.

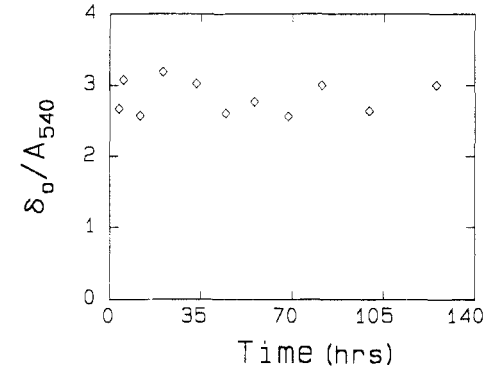

Figure 2. Absorbance-scaled birefringence amplitude, δ_0/A_{540}, as a function of time for sample B at $X_c = 0.37$.

titive in a region of $X_c \sim 0.35$–0.40. Figure 1 plots the time needed to reach the stationary state versus X_c. All extensive parameters, such as the scattered light intensity, the amplitude of birefringence, changed "exponentially" with a time constant τ of ~43 h. They all followed an empirical equation $Y(t) - Y(\infty) = A \exp(-t/\tau)$ where $Y(t)$ was an extensive parameter at time t and A was an amplitude constant. If the absorbance of the solution at $\lambda_0 = 540$ nm was used to scale the extensive values, time-independent relations could be obtained for both the scattered light intensity and the solution birefringence as displayed typically in Figure 2 for the time dependence of absorption-scaled birefringence amplitude, δ_0/A_{540}. The intensive parameters, however, such as diffusion coefficients, radius of gyration, were essentially time independent after an initial time period of ~0.5 h as shown typically in Figure 3 for the time dependence of rotational diffusion coefficient (D_R). If a filtration using a filter of a nominal pore size of 0.2 μm was employed before solutions of $X_c < 0.43$ reached the steady state, weakly scattered solutions could be obtained. But they soon became strongly scattered solutions again. The detailed study of the time dependence of P4BCMU in solution has been reported elsewhere.[34] In the present study all measurements were performed after the solution had reached the stationary state; e.g., we waited ~5–10 days after the sample preparation before commencement of experimental data acquisition.

III.2. Optical Absorption. Both samples A and B could be very quickly dissolved in chloroform to form yellow solutions with absorption maxima located at $\lambda_{max1}^A = 460$ nm and $\lambda_{max1}^B = 468$ nm, respectively. When toluene was added, additional peaks appeared with absorption maxima located (when $X_c \to 0$) at $\lambda_{max2}^A = 535$ nm

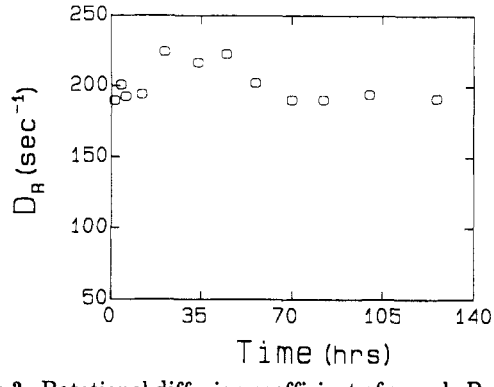

Figure 3. Rotational diffusion coefficient of sample B at $X_c = 0.37$ as a function of time. $C_{P4BCMU} = 1.2 \times 10^{-5}$ g/mL.

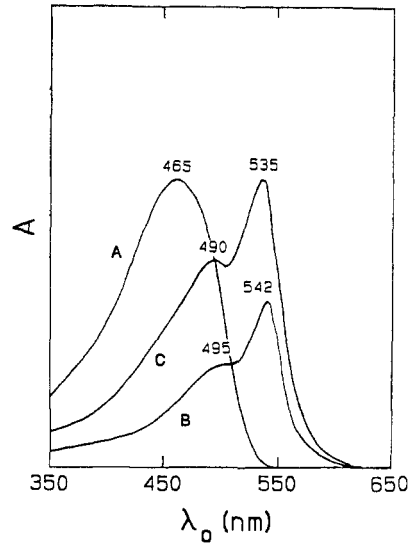

Figure 4. Typical absorption spectra for the two P4BCMU samples in different solvents: (A) sample A in chloroform; (B) sample B in toluene; (C) sample A in toluene. The ordinate (absorbance A) is in an arbitrary unit and not scaled for the three curves.

and $\lambda_{max2}^B = 542$ nm, respectively, and λ_{max1} was red-shifted by ~30 nm. Figure 4 shows typical absorption spectra of P4BCMU in chloroform and in toluene. The solution color thus would change gradually from yellow to orange or red depending on the ratio of A_{λ_2} to A_{λ_1}.

It is clear that there are two electronic configurations for P4BCMU in a mixed solvent. Analogous to Kuhn's modified free-electron quantum-mechanical theory for polyenes, the location of the absorption maximum for polydiacetylenes is related to the π-conjugation length by[49]

$$\Delta E = \frac{hc}{\lambda_0} = V_0 + \left(\frac{h^2}{mL_0^2} - \frac{V_0}{2}\right) \Big/ (2n + 1) \quad (9)$$

with c, V_0, h, m, L_0, and n being, respectively, the velocity of light in vacuo, the amplitude of the sinusoidal potential along the chain, Planck's constant, the mass of an electron, the repeat unit (one monomer) length, and the number of monomers in the π-conjugation. Taking $V_0 = 1.75$ eV for polyenes[20] and L_0 ($=L_{mono}$) = 4.8 Å for the monomeric unit length (two single bonds, one double bond, and one triple bond in the trans configuration),[26] we can compute the conjugated repeat units of $n_{\lambda=465} \approx 6$ and $n_{\lambda=542} \approx 11$. The longer conjugation state only appears when the solvent quality becomes poor. In the concentration range of our study (10^{-4}–10^{-6} g/g) Lambert–Beer's law is still valid for P4BCMU in solution. If A_{540} is scaled by the solution concentration, we could obtain information on the amount

Table II
Characteristics of P4BCMU in Chloroform/Toluene Solutions[f]

X_c	D_R, s^{-1}	D_T, 10^{-8} cm^2 s^{-1}	Var[a]	R_g,[b] nm	R_h,[c] nm	R_g/R_h	$[M_w(\partial n/\partial C)^2]_{X_c}/[M_w(\partial n/\partial C)^2]_{X_c=1}$
				Sample A[d]			
*0	24.5	2.14	0.04	229	190	1.20	1430
*0.10	76.0	2.60	0.08	145	150	0.97	600
0.30	146.0	3.44	0.06	117	111	1.06	500
0.36	205.0	4.60	0.06	80	86	0.93	370
*0.40	340.0	4.71	0.02	82	84	0.98	180
0.43	~4500	8.21	0.15	57	48	1.19	6
0.63		19.4	0.25	28	20	1.37	1
*1		23.8	0.31	25	17	1.48	1
				Sample B[e]			
0	14.5	1.84	0.04	268	220	1.22	56
0.35	71.0	2.55	0.14	158	158	1.00	
*1		4.87	0.34	120	84	1.43	1

[a] Var is variance from fittings of correlation functions either by the cumulants method or by CONTIN. [b] R_g values, which are only apparent in the solvent mixtures, have been corrected for anisotropy effect. [c] Equivalent hydrodynamic radius according to the Stokes–Einstein relation. [d] $(M_w)_A = 1.2 \times 10^5$ g/mol. [e] $(M_w)_B = 2.4 \times 10^6$ g/mol. [f] All values of the rows marked by asterisks have been extrapolated to infinite dilution. Values in the remaining rows are obtained from dilute solutions (typically $C = 1 \times 10^{-6}$ g/g for $X_c = 0$ and $C < 1 \times 10^{-5}$ for the rest) where particle sizes have been proven to be concentration independent.[21]

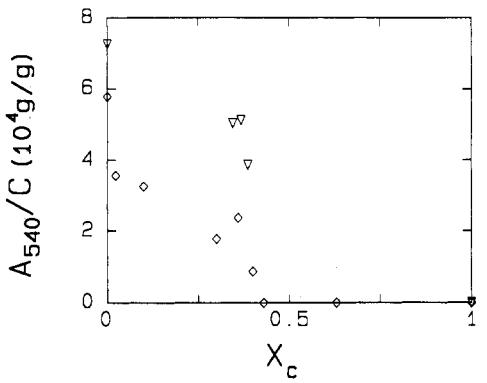

Figure 5. Concentration-scaled absorbance, A_{540}/C, as a function of X_c: diamonds, sample A; inverted triangles, sample B.

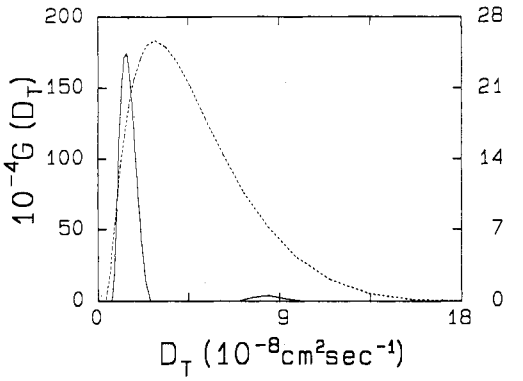

Figure 6. Distributions of translational diffusion coefficient (D_T) obtained from CONTIN fittings of autocorrelation functions of sample B measured by dynamic light scattering: (dashed line) $X_c = 1.0$, $C = 1.2 \times 10^{-4}$ g/g, $K^2 = 3.82 \times 10^9$ cm^{-2} ($\theta = 25°$) and the right ordinate, $\bar{D}_T = 4.9 \times 10^{-8}$ cm^2 s^{-1} and variance Var = 0.34; (solid line) $X_c = 0$, $C = 1.0 \times 10^{-6}$ g/g, $K^2 = 2.64 \times 10^9$ cm^{-1} ($\theta = 20°$) and the left ordinate; $\bar{D}_T = 1.5 \times 10^{-8}$ cm^2 s^{-1} and Var = 0.04 with the small hump (only 3% in total area) ignored.

of the longer conjugation formed, provided that the extinction coefficient ϵ_{540} remains unchanged. Figure 5 displays the scaled absorbance A versus the solvent composition. For both samples the conjugation change only happens when X_c is smaller than ~0.43; $A_{\tilde{5}40}$ continues to increase with decreasing chloroform content in the solvent mixture.

III.3. LLS Measurements. a. Characterization of the samples. Many studies have shown that P4BCMU molecules in chloroform are single coils. The coils do not have either strong scattering power or strong birefringence. From light-scattering measurements of P4BCMU in chloroform solutions we determined that the weight-averaged molecular weights M_w of sample A and sample B were 1.2×10^5 and 2.4×10^6 g/mol, respectively. The M_w value of sample A shows that sample A has possibly been photodegraded by random chain scission[20] during aging. Both samples show very broad molecular weight distributions (MWD). Figure 6 (dashed line) plots a distribution of translational diffusion coefficient D_T of sample B in chloroform from a small-angle dynamic LLS measurement of autocorrelation function by using the CONTIN algorithm. Figure 7 shows the corresponding MWD by using an empirical formula $D_T = k_D M^{-\alpha_D}$ with $k_D = 4.8 \times 10^{-4}$ and $\alpha_D = 0.61$ determined according to the procedure described in the Appendix. From the MWD of samples A and B we calculated $(M_w/M_n)_A = 2.2$ and $(M_w/M_n)_B = 2.1$.

b. Composition dependence of D_T and R_g. Following eq 1 and 2 and by extrapolation of concentration to infinite dilution and of scattering angle to zero scattering angle, the translational diffusion coefficient D_T can be computed

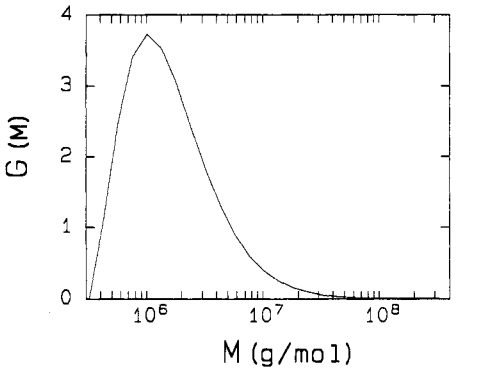

Figure 7. Molecular weight distribution of sample B in chloroform obtained from the D_T distribution (Figure 6, dashed line) according to the procedure described in the appendix with D_T (cm^2/s) = $k_D M^{-\alpha_D}$ (g/mol); $k_D = 4.8 \times 10^{-4}$ and $\alpha_D = 0.61$.

from the fitting of autocorrelation function and R_g obtained from the intensity data after an anisotropy correction. Depolarized LLS measurements showed a measurable anisotropy for P4BCMU in both good and poor solvents, e.g. the anisotropy factor $|\delta'| = 0.17$ for P4BCMU in chloroform, which would cause only a few percent corrections in measured M_w and R_g (see ref 42 for the computation procedures). The $|\delta'|$ value increased to 0.24,

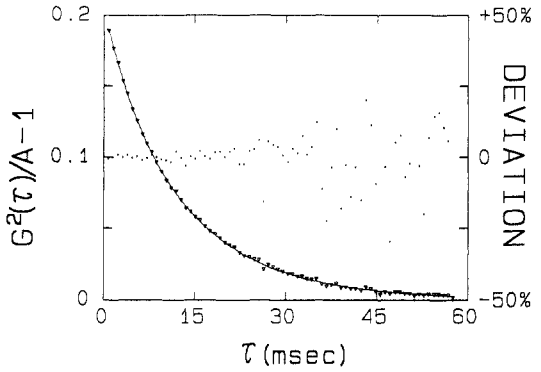

Figure 8. Unnormalized square electric field correlation function (inverted triangles) of sample B at $X_c = 0$, $C = 1 \times 10^{-6}$ g/g, and $\theta = 20°$ and the fitted curve from CONTIN (solid line) with the relative deviation [(data$_{meas}$ − data$_{calc}$)/data$_{meas}$] The corresponding distribution is shown in Figure 6 (solid line).

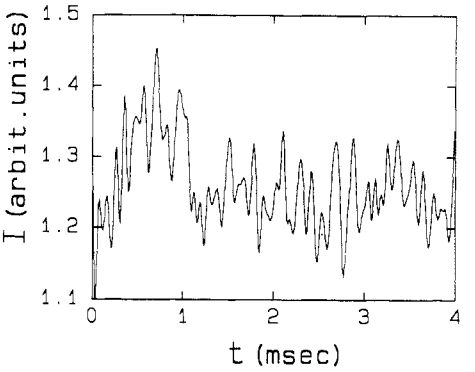

Figure 9. Birefringence trace from sample A in chloroform ($X_c = 1$) with a pulse width of 0.8 ms and an applied electric field strength of 6.7 kV/cm and $C_{P4BCMU} = 1 \times 10^{-3}$ g/mL. The ordinate is the absolute depolarized transmitted intensity. The noisy peak from $t \approx 0.3$ to ~1.1 ms corresponds to the weak but detectable birefringence from the polymer coils.

indicating more rod aggregates were formed as $X_c \to 0$. The polydispersity of P4BCMU in solution became surprisingly small when X_c was smaller than 0.43, i.e. when the solution color started to change, as listed in Table II (column Var) and shown typically in Figures 6 (solid line) and 8. By using the Stokes–Einstein formula to convert D_T to an equivalent hydrodynamic radius R_h, both R_g and R_h were continuously increased with varying ratios of R_g to R_h as the X_c value was decreased. As $X_c \to 0$, the scattered intensities from the solute per unit concentration were also increased up to 1430 and 56 times for samples A and B, respectively. These changes indicate that polymer molecules contain either intermolecular aggregation to have formed large aggregates or intramolecular straightening of the polymer chain with corresponding increases in the refractive index increment. These two mechanisms could be distinguished either from the molecular weight determination in which the value of refractive index increment ($\partial n/\partial C$) is crucial or by model fittings of characteristic parameters such as diffusion coefficients.

III.4. TEB Measurements. There were only very weak birefringence signals with very fast decay rates from P4BCMU in chloroform or in high X_c of chloroform/toluene mixtures as shown in Figure 9. For P4BCMU chloroform/toluene solutions with $X_c < 0.43$, there were strong birefringence signals when an applied field was turned on. The intensity of the depolarized transmitted light was solution concentration and solvent composition dependent, as well as electric pulse width and strength dependent. We were unable to reach the plateau region for the amplitude of birefringence due to the power supply and cell design limitations in our TEB instrument. The field-free relaxation rate also depended on the above variables, but for a given solution the relaxation rate reached a plateau either in relatively low fields or with short pulse widths. For example, the τ value (as defined in eq 4) of a sample B solution at $X_c = 0.37$ and $C = 1.2 \times 10^{-5}$ g/g remained the same with E (the electric field strength) > 1 kV/cm and pulse width >10 ms. By choosing proper pulse widths and electric field strengths, we have measured decay rates for various solutions in the plateau region where the characteristic decay time constant is reciprocally proportional to the rotational diffusion coefficient (D_R) of cylindrically anisotropic particles. The results are shown in column D_R of Table II.

IV. Discussions

Light scattering studies of P4BCMU in chloroform result in small values of both R_g and R_h. Since TEB measurements show only trace amounts of birefringence within our apparatus limitation, the molecules in solution are mostly coil-like with small geometrical dissymmetry. In Θ condition the value of $\langle R_h^{-1}\rangle_z \langle R_g^2\rangle_z^{1/2}$ is 1.732 for coils with the most probable distribution and 1.504 for uniform coils,[50] while our R_g/R_h ratio of 1.4 is typical for coils in a good solvent. By using neutron scattering at large scattering vectors ($K > 3 \times 10^5$ cm^{-1}), Rawiso et al.[22] have found that P4BCMU in a good solvent (toluene solution at high temperatures) is mainly trans configurational and rubber-band-like with a persistence length (ρ) of ~16 nm according to the Porod–Kratky wormlike chain model; the rigidity comes mainly from the π-conjugation not from the hydrogen bonding between the side groups. The mean-square radius of gyration of the chain cross section (R_c^2) is only 0.6 nm^2, which is much smaller than the fully extended side-chain length. If we are to use the Porod–Kratky model, the persistence length could be fitted out from equations of $D_T(\rho)$ or $R_g(\rho)$. But for our polydispersed samples the molecular weight distribution (MWD) has to be taken into account. The calculation will run into some difficulties in the iterative fitting procedure, even if we known the MWD. If we make an assumption that the molecular weight distribution is Schulz type, then in the case of $M_w/M_n = 2$, the square z-averaged radius of gyration will approximately be

$$\langle R_g^2\rangle_z = \int R_g^2(P)\, P^\alpha \exp\left(-\frac{\alpha P}{P_w}\right) dP \Big/ \int P^\alpha \exp\left(-\frac{\alpha P}{P_w}\right) dP \quad (10)$$

where $\alpha = (1 - M_n/M_w)^{-1}$ and $R_g(P)$ and P_w are the radius of gyration of polymer of polymerization number P and the weight-averaged polymerization number, respectively. According to the equation for the radius of gyration of wormlike chains[51]

$$R_g^2(P) = \tfrac{1}{3}\rho^2 x[1 - (3/x^3)(x^2 - 2x + 2 - 2e^{-x})] \quad (11)$$

with $x = L/\rho$ and L being the contour length, which could be calculated using $L = Pl$ with l (=4.8 Å) being the monomer (4BCMU) length of the trans configuration. When the values of $(M_w/M_n)_A = 2.2$ and $(M_w/M_n)_B = 2.1$ are used, the fittings for both samples A and B show the persistence length ρ to be 16 nm in very good agreement with the result reported by Rawiso et al. It is noticeable that even though sample A has 20 times the molecular weight of sample B, their persistence lengths are the *same*, which is coincident with the optical absorption observation where the two samples have very close absorption maxima. When the computation that each conjugation consists of

six repeating monomer units is used, a persistence length should include ~5–6 kinks of the π-conjugation.

A previous study[22] showed that when the solvent condition became poor (toluene solution at low temperatures), the polymers were aggregated in three dimension with an increasing value of mass per unit length. The aggregation number was ~30 for a P4BCMU sample with M_w = 1.7 × 10^6 g/mol in toluene at room temperature; no anisotropy in scattering was observed. The aggregates had a well-defined geometry, which could be presented by a so-called fringed micelle model. Our studies as listed in Table II demonstrate that when X_c < 0.43 P4BCMU in chloroform/toluene solutions the color starts to change and the size becomes bigger and bigger, as $X_c \rightarrow 0$.

During the sample clarification procedures for LLS measurements, we noticed that for the solutions of different X_c values the maximum rotation speed allowed to prevent the red substance from depositing on the wall of the centrifuge tube was greatly reduced with decreasing X_c. For example, when X_c = 1, we could use a speed corresponding to the centrifuging force of 1.2 × 10^4 g without causing any solution inhomogeneity. But for X_c = 0, even in a concentration of 10^{-6} g/g only a very low rotation speed corresponding to a centrifuging force of 30g for 2 h could be used without disturbing the solution. The phenomena observed during centrifugation were a strong indication of aggregation.

Our LLS measurements were performed over a small KR_g region (KR_g < 1.5) where the correct R_g and D_T values of an individual scatterer could be obtained without appreciable distortions from internal structures.

Our TEB measurements display a constant relaxation rate with a strong birefringence signal for a given sample over a range of pulse widths and field strengths. This observation implies that the particles (tentatively, we call them particles, they could be either single molecules or aggregates) must be less flexible, otherwise the relaxation rate should decrease if the particles were stretched. We have tried several common rigid models, such as a rigid rod or ellipsoids of revolution, to fit our data. We have, for each solvent composition, three independently measured values, D_R, D_T, and R_g. For rigid cylindrically symmetric models, only two of these values are needed to find out the two parameters (cylinder length and diameter). Thus, we can couple any two among the three variables in order to confirm the validity of a particular model. As shown in Figures 6 (solid line) and 8 and listed in Table II, the size distributions become very narrow once the strong scatterers are formed. Thus, in a first-order approximation of uniform particle sizes in these solutions, there is no need to take into account of the polydispersity effect and to use different averages when doing such a comparison with different geometrical models. For a rigid straight rod, the following equations were used[52,53]

$$R_g^2 = \frac{L^2}{12}\left(1 + \frac{3}{2r^2}\right) \tag{12}$$

$$D_R = \frac{3k_BT}{\eta_0\pi L^3}\left(\ln(2r) - \left[1.57 - 7\left(\frac{1}{\ln(2r)} - 0.28\right)^2\right]\right) \tag{13}$$

$$D_T = \frac{k_BT}{3\pi\eta_0 L}\left(\ln(2r) - \frac{1}{2}\left[1.46 - 7.4\left(\frac{1}{\ln(2r)} - 0.34\right)^2 - 4.2\left(\frac{1}{\ln(2r)} - 0.39\right)^2\right]\right) \tag{14}$$

with L, η_0, k_B, and T being, respectively, the length, the solvent viscosity, the Boltzmann constant, and the absolute temperature and r being the ratio of the length (L) to the diameter (D). And for a prolate ellipsoid[52,54]

$$R_g^2 = \frac{L^2}{20}\left(1 + \frac{2}{r^2}\right) \tag{15}$$

$$D_R = \frac{3k_BTr^3}{2\pi\eta_0 L^3(r^4 - 1)}\left(\frac{2r^2 - 1}{(r^2 - 1)^{1/2}}\ln\left[r + (r^2 - 1)^{1/2}\right] - r\right) \tag{16}$$

$$D_T = \frac{k_BTr}{3\pi\eta_0 L(r^2 - 1)^{1/2}}\ln\left[r + (r^2 - 1)^{1/2}\right] \tag{17}$$

with L being the length of the long axis and r being the ratio of the long axis to the short axis.

Table III
Rigid Model Representations of P4BCMU in Solution

	rod				prolate ellipsoid			
	(D_T, R_g)		(D_T, D_R)		(D_T, R_g)		(D_T, D_R)	
	L, μm	D, μm	L, μm	D, μm	L, μm	D, μm	L, μm	D, μm
				Sample A				
0	0.77	0.091	0.73	0.098	1.00	0.15	0.75	0.21
0.10	0.48	0.098	0.45	0.11	0.60	0.17	0.38	0.27
0.30	0.40	0.070	0.37	0.074	0.50	0.11	0.35	0.17
0.36	0.27	0.057	0.37	0.041	0.32	0.11	0.39	0.084
0.40	0.28	0.053	0.29	0.051	0.34	0.095	0.28	0.12
				Sample B				
0	0.92	0.11	0.88	0.11	1.18	0.17	0.92	0.22
0.35	0.53	0.094	0.47	0.11	0.66	0.17	0.39	0.27

Table IV
Wormlike Chain Model Fitting of P4BCMU in Solution

	sample A				sample B			
X_c	0	0	0.1	0.3	0.4	0	0	0.35
b (prefixed), Å	53	80	80	80	80	53	80	80
L, μm	0.99	1.05	0.63	0.53	0.35	1.12	1.16	0.77
ρ, μm	0.38	0.30	0.23	0.16	0.14	0.53	0.44	0.17
a', μm	0.13	0.13	0.16	0.11	0.087	0.16	0.15	0.15

Table III lists the fitting results by using the IMSL subroutine ZREAL1 with a fitting precision (relative error residue) down to 10^{-4} from different pairs among D_R, D_T, and R_g to the rod and prolate ellipsoid models. The fittings from the rod model give reasonable self-consistent results. The choice of either data pairs (from D_T and R_g or from D_R and D_T) only causes a difference of ~10% for most fittings. The lengths from the two samples are very close (L_B is only ~15% longer than L_A) in the case of the pure toluene solution, although sample B has 20 times the molecular weight of sample A. Due to the difference in shape at the ends, the prolate ellipsoid model yields a smaller L/D ratio than the rod model. An oblate ellipsoid model has also been tried, but it could not produce meaningful results. From Table III the particles are much fatter than if they were fully stretched molecules, which should have a diameter of only 40 Å, and they are longer (sample A) and shorter (sample B) than a fully stretched molecule, which should be 0.1 μm (sample A) or 2.2 μm (sample B) in length, respectively. Thus, the possibility for particles in orange or red solutions being single molecules should be ruled out. Although single molecules of sample A and of sample B are different in molecular weight, after aggregation they tend to form particles that have similar size and shape. Also, as shown in Table III, the growth of both diameter and length of particles, as X_c becomes smaller, is another evidence for aggregation.

Another possible semirigid rod model would be a bending (or wormlike) rod, whose corresponding equations

could be found as follows (and eq 11)[55,56]

$$D_R = \frac{k_B T}{2\eta_0 x^2 \rho^3}\left(0.506\sqrt{x} - 0.636 \ln (b/2\rho) - 1.548 + 0.64\frac{b}{a'}\right) \quad (18)$$

$$D_T = \frac{k_B T}{3\pi\eta_0 x\rho}\left(A_1(0.5x)^{1/2} + A_2 + \frac{A_3}{(0.5x)^{0.5}} + \frac{A_4}{0.5x} + \frac{A_5}{(0.5x)^{1.5}}\right) \quad x > 4.556 \quad (19)$$

$$D_T = \frac{k_B T}{3\pi\eta_0 x\rho}\left(C_1 \ln\left(\frac{x\rho}{a'}\right) + C_2 + C_3\frac{x}{2} + C_4\left(\frac{x}{2}\right)^2 + C_5\left(\frac{x}{3}\right)^3 + C_6\left(\frac{a'}{x\rho}\right)\ln\left(\frac{x\rho}{a'}\right) + C_7\left(\frac{a'}{x\rho}\right) + C_8\left(\frac{a'}{x\rho}\right)^2 + C_9\left(\frac{a'}{x\rho}\right)^3 + C_{10}\left(\frac{a'}{x\rho}\right)^4\right) \quad x \le 4.556 \quad (20)$$

with $x = L/\rho$, and L, b, ρ, and a' being the contour length, the distance between adjacent frictional elements, the persistence length, and the Stokes diameter of an element, respectively. In eq 19 and 20, $A_1 - A_5$ and $C_1 - C_{10}$ are all functions of (a'/ρ).[56] We have four floating parameters, x, ρ, b, and a', in three equations. Again, if the particle is a (partially) straightened molecule, then a' would be close to twice the side-chain length (~40 Å) and b could be reasonably chosen as the length of the longer π-conjugation, which is about 53 Å. But that is not the case. If we prefix the b value being 53 Å, the sets of x, ρ, and a' obtained have much thicker diameters of ~150 nm as shown in Table IV. This result again rules out the single-chain phenomenon in poorer solvents.

During the iterative fittings it was found that for all the data sets there was only a limited range available for prefixed b values, which could be used while still obtaining stable and meaningful solutions (sets of L, ρ, and a'). This range is from ~40 to ~110 Å. For a particular set of D_R, D_T, and R_g, a' is quite stable, but increasing L (up to ~15% bigger) and decreasing ρ (down to ~40% smaller) were found when b was increased from 40 to 110 Å. Table IV lists the values using a prefixed b of 80 Å. The results are surprisingly close to those from the rod model. Although we started with a wormlike chain model, P4BCMU in these solutions was found to be fairly rigid, with a typical L/ρ value being only 2–4.

The scattered intensity ratio for solutions with $X_c < 1$ when compared with chloroform solutions ($X_c = 1$), as the values listed in the last column of Table II, originates from both the change in the refractive index increment $(\partial n/\partial C)$ of the solution and/or the aggregation of polymer molecules. Thus, the $\partial n/\partial C$ values are crucial in the determination of the aggregation number. Muller et al.[25] have extensively measured $\partial n/\partial C$ values for P4BCMU in toluene at various concentrations and wavelengths. They concluded that the value for P4BCMU in toluene at λ_0 = 633 nm was only about twice the value for P4BCMU in chloroform. Due to the different refractive indices of toluene and chloroform and their different boiling points, measurements of refractive index increment for solutions in mixed solvents could not provide us with reliable values. So, we emphasize only the toluene solution. If we use the value of $(\partial n/\partial C)_{X_c=0} = 0.242$ and assume that it is independent of the molecular weight of P4BCMU, then the average aggregation numbers are readily estimated for P4BCMU in toluene; $n_A = 360$ and $n_B = 14$. In the same solvent condition (e.g. $X_c = 0$), the aggregation number of sample A is much higher than sample B. As reported and suggested before (ref 35 and the references therein), the neutral coil of polydiacetylene in a poor solvent (or solvent mixture) would be partially straightened to have longer π-conjugation; meanwhile, the molecules could become charge carriers in a solvent of a proper dielectric constant. The charge density (ρ_e) is reciprocally proportional to the polymerization number, and charges are mainly located at the ends of the molecules (ref 35 and the references therein). Under electrostatic and solvation forces, those charged molecules would aggregate to form rodlike particles. According to this explanation, sample A would have a higher charge density than sample B and be easier to adhere with each other. Also, the structure of aggregates from sample A should be denser. Thus in a stationary (equilibrium) state, sample A is expected to have a higher aggregation number and denser structure. This explains the result of the aggregates from sample A having a large aggregation number ($n_A = 360$ vs $n_B = 14$ corresponding to $M_{w,A} = 4.3 \times 10^7$ g/mol vs $M_{w,B} = 3.4 \times 10^7$ g/mol) but at smaller dimensions ($(R_g)_A = 229$ nm vs $(R_g)_B = 268$ nm) than those from sample B. When the above aggregation numbers for sample A and sample B are combined with the aggregation number reported by Rawiso et al.,[22] a linear empirical relation between the average polymerization number P_w and the aggregations number n in toluene, $(n - 1) \approx 8.5 \times 10^4 P_w^{-1} \propto \rho_e$ (charge density), could be extracted. The reasons for the different molecular weight samples approaching similar size and shape are still not clear. The narrower size distribution for the rod aggregates does suggest a closed association of micelle formation for P4BCMU in poor solvent.

V. Conclusion and Remarks

By LLS and TEB measurements and model fittings of measured data, we have experimentally confirmed that P4BCMU polymer molecules in good and poor solvent exist in single wormlike chains and uniform rodlike aggregates, respectively. The concentration dependence of particle size in dilute solution is very weak. This finding agrees with previous results.[21,22] The aggregation number is molecular weight and solvent composition dependent. The transformation (color and size change) starts at $X_c \lesssim 0.43$. The size of aggregates varies with solvent composition. The monodisperse behavior of aggregates suggests that the aggregation process might be micellization-like. Further investigation of the transition of polydiacetylene in solution over a much shorter time range is needed to clarify the transition mechanism.

Acknowledgment. We thank Drs. R. R. Chance and D. G. Peiffer who provided us the polydiacetylene samples. This work was supported by the Polymers Program of the National Science Foundation (DMR8617820).

Appendix

Conversion of D_T Distribution to M Distribution. By using the relation $D_T = k_D M^{-\alpha_D}$ with k_D and α_D being two scaling constants, we can convert the translational diffusion coefficient (D_T) distribution to the molecular weight (M) distribution as follows.

The discrete normalized linewidth distribution from photon correlation is

$$\sum F(\Gamma_i) = \sum \frac{N_i M_i^2}{\sum N_i M_i^2} = 1 \quad (A1)$$

where N_i, M_i, and Γ_i ($=K^2 D_{T,i}$, K is the magnitude of the scattering vector) are the numbers of molecules, the mo-

lecular weight, and the linewidth, respectively, of the ith species. Substituting eq A1 into the definition of the weight-averaged molecular weight (M_w), we get

$$M_w = \frac{\sum F(M_i)}{\sum F(M_i)/M_i} = \frac{\sum N_i M_i^2}{\sum N_i M_i} = \frac{\sum N_i M_i^2}{\sum (F(\Gamma_i)[\sum N_i M_i^2]/M_i)} = \left(\sum \frac{F(\Gamma_i)}{M_i}\right)^{-1} \quad \text{(A2)}$$

McWhirter and Pike[57] have showed that the behavior of a logarithmically spaced discrete distribution $F(\Gamma_i)$ could be equalized to a continuous distribution $G(\Gamma)$ after each point of $F(\Gamma_i)$ is corrected by multiplying a factor Γ_i^{-1}; i.e. $F(\Gamma_i) = \Gamma_i G(\Gamma_i)$. Thus, in a logarithmically spaced continuous distribution from the CONTIN algorithm, eq A2 could be rearranged to yield

$$M_w = \frac{k_D^{1/\alpha_D} \sum G(\Gamma_i)\Gamma_i}{\sum G(\Gamma_i) D_i^{1/\alpha_D} \Gamma_i} = (K^2 k_D)^{1/\alpha_D} \frac{\sum G(\Gamma_i)\Gamma_i}{\sum G(\Gamma_i)\Gamma_i^{1/\alpha_D+1}} \quad \text{(A3)}$$

The left side of eq A3 could be determined by using static LLS. α_D can then be obtained from a ratio of two samples of different molecular weight

$$\frac{M_{w1}}{M_{w2}} = \left(\frac{\sum G(\Gamma_i)\Gamma_i}{\sum G(\Gamma_i)\Gamma_i^{1/\alpha_D+1}}\right)_1 \left(\frac{\sum G(\Gamma_i)\Gamma_i^{1/\alpha_D+1}}{\sum G(\Gamma_i)\Gamma_i}\right)_2 \left(\frac{K_1}{K_2}\right)^{2/\alpha_D} \quad \text{(A4)}$$

With α_D, k_D can be determined from eq A3.

Following a similar route, M_n can be calculated by

$$M_n = \frac{\sum N_i M_i}{\sum N_i} = \frac{\sum F(\Gamma_i)/M_i}{\sum F(\Gamma_i)/M_i^2} = (k_D K^2)^{1/\alpha_D} \frac{\sum G(\Gamma_i)\Gamma_i^{1/\alpha_D+1}}{\sum G(\Gamma_i)\Gamma_i^{2/\alpha_D+1}} \quad \text{(A5)}$$

The continuous MWD, $G(M)$, is related to $G(\Gamma)$ according to the relation

$$G(M) = \Gamma G(\Gamma)/M \quad \text{(A6)}$$

References and Notes

(1) Matsuda, H.; Nakanishi, H.; Kato, S.; Kato, M. *J. Polym. Sci., Polym. Chem. Ed.* **1987**, *25*, 1663.
(2) Wegner, G. *Z. Naturforsch.* **1969**, *24B*, 824; *Makromol. Chem.* **1972**, *154*, 35.
(3) Baughman, R. H.; Chance, R. R. *J. Polym. Sci., Polym. Phys. Ed.* **1976**, *14*, 2037.
(4) Patel, G. N. *Polym. Prepr. (Am. Chem. Soc., Div. Polym. Chem.)* **1978**, *19*, 154.
(5) *Nonlinear Optical Properties of Organic Polymeric Materials*; Williams, D. J., Ed.; ACS Symposium Series 233; American Chemical Society: Washington DC, 1983. *Crystallography of Ordered Polymers*; Sandman, D. J., Ed.; ACS Symposium Series 337; American Chemical Society: Washington, DC, 1987.
(6) Polydiacetylene. NATO Advanced Science Institutes Series E: Applied Science; Bloor, D., Chance, R. R., Eds.; Martinus Nijheff Publishers: Dordrecht, The Netherlands, 1985; Vol. 102.
(7) *Advanced Nonlinear Polymer Inorganic Crystallography Liquid Crystallography, Laser Media*; Musikant, S., Ed. Proceedings of SPIE–The International Society of Optical Engineering; SPIE–The International Society for Optical Engineering: Bellingham, WA, 1988; Vol. 824.
(8) *Synthetic Metals*; Proceedings of the International Conference on the Science and Technology of Synthetic Metals; Heeger, A. J., Ed.; Elsevier: Sequoia, The Netherlands, 1987; Vol. 18, pp 1–3.
(9) Marrian, C. R. K.; Colton, R. J.; Snow, A.; Taylor, C. J. *Mater. Res. Soc. Symp. Proc.* **1987**, *76*, 353.
(10) Korshak, Y. V.; Medvedeva, T. V.; Ovchinnikov, A. A.; Spektor, V. N. *Nature (London)* **1987**, *326*, 370.
(11) Shutt, J. D.; Rickert, S. E. *Langmuir* **1987**, *3*, 460.
(12) Baughman, R.; Chance, R. R. *Polym. Prepr. (Am. Chem. Soc., Div. Polym. Chem.)* **1986**, *27*, 67.
(13) Prusik, T.; Montesalvo, M.; Wallace, T. *Radiat. Phys. Chem.* **1988**, *31*, 441.
(14) Singh, B. P.; Prasad, P. N. *J. Opt. Soc. Am. B: Opt. Phys.* **1988**, *5*, 453.
(15) Sasaki, K.; Pujii, K.; Tomioka, T.; Kinoshita, T. *J. Opt. Soc. Am. B: Opt. Phys.* **1988**, *5*, 457.
(16) Hanamura, E.; Itsubo, A. *Proc. SPIE-Int. Soc. Opt. Eng.* **1988**, *824*, 66.
(17) Peiffer, D. G.; Chung, T. C.; Schulz, D. N.; Agarwal, P. K.; Garner, R. T.; Kim, M. W. *J. Chem. Phys.* **1986**, *85*, 4712.
(18) Lim, K. C.; Kapitulnik, A.; Zacher, R.; Heeger, A. J. *J. Chem. Phys.* **1985**, *82*, 516.
(19) Patel, G. N.; Chance, R. R.; Witt, J. D. *J. Chem. Phys.* **1979**, *70*, 4387.
(20) Wenz, G.; Mueller, M. A.; Schmidt, M.; Wegner, G. *Macromolecules* **1984**, *17*, 837.
(21) Lim, K. C.; Heeger, A. J. *J. Chem. Phys.* **1985**, *82*, 522.
(22) Rawiso, M.; Aime, J. P.; Fave, J. L.; Schott, M.; Muller, M. A.; Schmidt, M.; Baumgartl, B.; Wegner, G. *J. Phys. Fr.* **1988**, *49*, 861.
(23) Patel, G. N.; Khanna, Y. P. *J. Polym. Sci., Polym. Phys. Ed.* **1980**, *18*, 2209.
(24) Wenz, G.; Wegner, G. *Makromol. Chem., Rapid Commun.* **1982**, *3*, 231.
(25) Muller, M. A.; Schmidt, M.; Wegner, G. *Makromol. Chem., Rapid Commun.* **1984**, *5*, 83.
(26) Allegra, G.; Bruckner, S.; Schmidt, M.; Wegner, G. *Macromolecules* **1986**, *19*, 399.
(27) Coyne, L. D.; Chang, C.; Hsu, S. L. *Makromol. Chem.* **1987**, *188*, 2311; **1987**, *188*, 2679.
(28) Chance, R. R.; Patel, G. N.; Witt, J. D. *J. Chem. Phys.* **1979**, *71*, 206.
(29) Dobrosavljevic, V.; Stratt, R. M. *Phys. Rev. B: Condens. Matter* **1987**, *35*, 2781.
(30) Kollmar, C.; Sixl, H. *J. Chem. Phys.* **1987**, *87*, 1396; **1988**, *88*, 1343.
(31) Kuzmany, H.; Kuerti, J. *Synth. Met.* **1987**, *21*, 95.
(32) Bredas, J. L.; Chance, R. R.; Baughman, R. H.; Silbey, R. *J. Chem. Phys.* **1982**, *76*, 3673.
(33) Schweizer, K. S. *Chem. Phys. Lett.* **1986**, *125*, 118.
(34) Chu, B.; Xu, R. In *Proc. ELECTROPTO88*, in press.
(35) Xu, R.; Chu, B. *Macromolecules*, submitted for publication.
(36) Peiffer, D. G., personal communication.
(37) Patel, G. N.; Chance, R. R.; Witt, J. D. *J. Polym. Sci., Polym. Lett. Ed.* **1978**, *16*, 607.
(38) Zhou, Z.; Chu, B. *J. Colloid Interface Sci.* **1988**, *126*, 171.
(39) Koppel, D. E. *J. Chem. Phys.* **1972**, *57*, 4814.
(40) Provencher, S. W. *Comput. Phys. Commun.* **1982**, *27*, 213; **1982**, *27*, 229.
(41) Berry, G. C. *J. Polym. Sci., Polym. Symp.* **1978**, *65*, 143.
(42) Chu, B.; Xu, R.; DiNapoli, A. *J. Colloid Interface Sci.* **1987**, *116*, 182.
(43) Xu, R.; Ford, J.; Chu, B. In *Particle Size Distribution: Assessment and Characterization*; Provder, T., Ed.; ACS Symposium Series 332; American Chemical Society: Washington, DC, 1987; pp 115–132.
(44) DiTusa, M. R.; Schilt, A. A. *J. Chem. Educ.* **1985**, *62*, 541.
(45) Huglin, M. B., Ed. *Light Scattering from Polymer Solutions*; Academic Press: New York, 1972.
(46) Riddick, J. A.; Bunger, W. B.; Sakano, T. K. *Organic Solvents, Techniques of Chemistry*; Weissberger, A., Ed.; Wiley: New York, 1986; Vol. II.
(47) Chu, B.; Xu, R.; Maeda, T.; Dhadwal, H. S. *Rev. Sci. Instrum.* **1988**, *59*, 716.
(48) Chu, B.; Xu, R. *OSA Proc. Photon Corre. Tech. Appl.*, in press.
(49) Kuhn, H. *J. Chem. Phys.* **1949**, *17*, 1198.
(50) Kajiwara, K.; Burchard, W. *Polymer* **1981**, *22*, 1621.
(51) Hermans, J., Jr.; Hermans, J. J. *J. Phys. Chem.* **1958**, *62*, 1543.
(52) Broersma, S. *J. Chem. Phys.* **1960**, *32*, 1626.
(53) Newman, J.; Swinney, H. L.; Day, L. A. *J. Mol. Biol.* **1977**, *116*, 593.
(54) Tanford, C. *Physical Chemistry of Macromolecules*; Wiley: New York, 1961; p 237.
(55) Hearst, J. E. *J. Chem. Phys.* **1963**, *38*, 1062.
(56) Yamakawa, H.; Fujii, M. *Macromolecules* **1973**, *6*, 407.
(57) McWhirter, J. G.; Pike, E. R. *J. Phys. A: Math. Gen.* **1978**, *11*, 1729.